ChemPubSoc Europe

DOI: 10.1002/cbic.201402377

Single-Molecule Imaging Reveals that Small Amyloid-β_{1-42} Oligomers Interact with the Cellular Prion Protein (PrP^C)

Kristina A. Ganzinger,[a] Priyanka Narayan,[a, b] Seema S. Qamar,[c] Laura Weimann,[a] Rohan T. Ranasinghe,[a] Adriano Aguzzi,[d] Christopher M. Dobson,[a] James McColl,*[a, e] Peter St. George-Hyslop,*[c] and David Klenerman*[a]

Oligomers of the amyloid-β peptide (Aβ) play a central role in the pathogenesis of Alzheimer's disease and have been suggested to induce neurotoxicity by binding to a plethora of cell-surface receptors. However, the heterogeneous mixtures of oligomers of varying sizes and conformations formed by Aβ42 have obscured the nature of the oligomeric species that bind to a given receptor. Here, we have used single-molecule imaging to characterize Aβ42 oligomers (oAβ42) and to confirm the controversial interaction of oAβ42 with the cellular prion protein (PrP^C) on live neuronal cells. Our results show that, at nanomolar concentrations, oAβ42 interacts with PrP^C and that the species bound to PrP^C are predominantly small oligomers (dimers and trimers). Single-molecule biophysical studies can thus aid in deciphering the mechanisms that underlie receptor-mediated oAβ-induced neurotoxicity, and ultimately facilitate the discovery of novel inhibitors of these pathways.

For decades, research on the molecular basis of Alzheimer's disease (AD) has focused on the molecular component of the plaques characteristic of the disease, that is, highly structured, fibrilized amyloid-β (Aβ) peptide species. Although soluble Aβ oligomers (oAβ) have now emerged as the key neurotoxins in AD,[1–3] how exactly they disrupt and impair neuronal function is still a topic of active research. Alongside the view that toxicity is caused directly by oAβ interacting with and inserting into cell membranes,[4–6] receptor-mediated mechanisms of toxicity have been suggested; among the numerous putative targets are the RAGE, NMDA, glutamate, insulin, and human LilrB2 receptors,[7,8] as well as the cellular prion protein (PrP^C).[9] Since the initial discovery of PrP^C as a high-affinity receptor for Aβ42, numerous studies have confirmed the existence of a PrP^C–Aβ42 peptide interaction in vitro,[9–13] but have debated its contribution to the neurotoxicity and memory deficits characteristic of AD.[12–20] As with most of the identified Aβ receptors, PrP^C was found to bind oAβ with much higher affinity than monomeric Aβ (mAβ). However, oAβ assemblies typically exist as heterogeneous mixtures of oligomers of varying sizes and conformational states, and hence it is still a matter of debate as to which species within such ensembles interacts with PrP^C.[7,21] Indeed, the lack of methods to characterize oligomeric species that bind putative receptors presents a major hurdle to understanding AD, as emphasized by three recent reviews.[7,22,23] In this study, we used total internal reflection microscopy (TIRFM) to address this problem. We characterized the interaction between endogenous PrP^C and oAβ42 at the single-molecule level on the surface of live hippocampal cells, and investigated whether oligomers of a specific size (or from a specific preparation) bind preferentially to PrP^C.

In order to characterize the composition of oligomeric mixtures of Aβ42 in solution before addition to hippocampal cells, we used confocal two-color coincidence detection (cTCCD, Figure 1A). In this technique, two lasers are focused onto the same spot, thereby resulting in overlapping diffraction-limited confocal volumes, which are slowly scanned through a solution containing diffusing Aβ42 monomers and oligomers. In order to generate dual-labeled species upon oligomerization, we aggregated a mixture of Aβ42 peptides tagged at the N terminus with either HiLyte Fluor 488 or HiLyte Fluor 647. Oligomers are thus distinguished from monomers by the presence in both detection channels of simultaneous fluorescent signals, the intensity of which can be used to estimate the oligomerization order of the dual-labeled species (by comparison with the signal emitted by singly labeled monomeric species). We and others have investigated the effect of these labels on the aggregation of Aβ(1–40), and showed that HiLyte Fluor 647 does not affect the kinetics of fibril formation and that neither label affects the rate of monomer consumption during aggregation,

[a] K. A. Ganzinger,[+] Dr. P. Narayan,[+] Dr. L. Weimann, Dr. R. T. Ranasinghe, Prof. C. M. Dobson, Dr. J. McColl, Prof. D. Klenerman
Department of Chemistry, University of Cambridge
Lensfield Road, Cambridge, CB2 1EW (UK)
E-mail: dk10012@cam.ac.uk

[b] Dr. P. Narayan[+]
Present address: Whitehead Institute for Biomedical Research
9 Cambridge Center, Cambridge, MA 02142 (USA)

[c] Dr. S. S. Qamar,[+] Dr. P. St. George-Hyslop
Department of Clinical Neurosciences
Cambridge Institute for Medical Research, University of Cambridge
Cambridge CB2 0XY (UK)
E-mail: phs22@cam.ac.uk

[d] Prof. A. Aguzzi
UniversitätsSpital Zürich, Institut für Neuropathologie
Schmelzbergstrasse 12, 8091 Zürich (Switzerland)

[e] Dr. J. McColl
Present address: School of Biological Sciences, University of East Anglia
Norwich Research Park, Norwich NR4 7TJ (UK)
E-mail: J.Mccoll@uea.ac.uk

[+] These authors contributed equally to this work.

Supporting information for this article is available on the WWW under http://dx.doi.org/10.1002/cbic.201402377.

A)

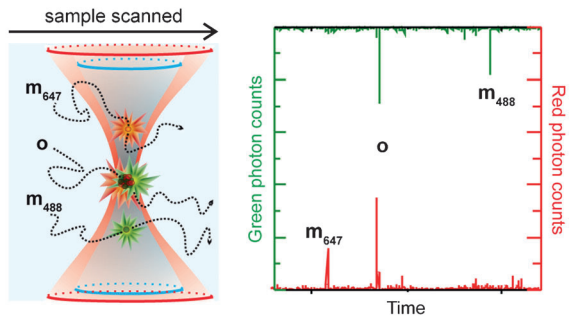

B)

Preparation method	Oligomeric fraction of Aβ (oAβ)	di– to tetramers [fraction of oligomeric Aβ]	penta– to decamers [fraction of oligomeric Aβ]	11– to 50-mers [fraction of oligomeric Aβ]
Sample from midway aggregation (AGG)	0.027±0.005	0.64±0.11	0.23±0.07	0.10±0.02
Amyloid-derived diffusible ligands (ADDL)	0.010±0.006	0.62±0.17	0.31±0.15	0.07±0.03

Figure 1. Characterization of AGG and ADDL Aβ oligomer preparations by cTCCD. A) cTCCD experiment. Aβ42 monomers labeled with HiLyte Fluor 488 ($\mathbf{m_{488}}$) and 647 ($\mathbf{m_{647}}$), and oAβ42 (**o**, containing both monomer types) diffuse through the confocal volume (left), which is scanned across the sample. Asynchronous fluorescent signals (events) are recorded in the green and red channels for oAβ42 monomers (synchronous signals are coincident events; right). B) Oligomeric fractions and size distributions of oAβ42 for both preparation methods as determined by cTCCD (25 pM sample concentration). Oligomeric fraction is the number of oAβ42 events divided by total events. From this fraction, the oAβ42 concentration in subsequent experiments was calculated (i.e., for oligomer preparations of 500 nM total peptide concentration: 4.9±2.9 nM (AGG), 13.7±2.3 nM (ADDL)). Calculated size distribution is detailed in the Methods section in the Supporting Information. There is no significant difference in oligomeric distributions between AGG and ADDL preparations (two sample independent t-test). All values are mean±SD, $n=3$.

or the morphology of the resulting fibrils.[24,25] We have previously validated the cTCCD method for the study of Aβ oligomerization by showing that time courses of monomer consumption during aggregation measured by cTCCD and by quantitative western blotting are in good agreement.[24] Because reconciling the results from experiments using different preparation methods has been a major challenge in the field of Aβ research,[23] we investigated the effect of the oAβ42 preparation method on the oAβ42–PrP^C interaction by comparing two different Aβ42 aggregation protocols. The first involves the extraction of samples from an aggregating mixture of Aβ42 under fibril-forming conditions ("AGG"); we and others have previously shown this to generate well-defined populations of oligomeric species.[24,26] The second method requires incubation of monomeric peptide solutions at low temperatures for long periods (16–24 h) to produce stable preparations of amyloid-derived diffusible ligands ("ADDL") and protofibrils, which have been used in many studies.[9,10,12,13,27] We used the modified protocol for ADDL preparation of Laurén et al.[9] to allow direct comparison of our results with previous studies. Although AGG and ADDL protocols use different Aβ concentrations in the aggregation step (10 and 40 μM, respectively), both preparations were diluted to a total peptide concentration of 25 pM immediately prior to cTCCD measurements, in order to minimize multiple occupancy of the femtoliter-sized confocal volumes. cTCCD characterization showed that both aggregation protocols produce detectable oligomers (1–3% of the total number of peptide assemblies, or ~8% of total peptide mass; Figure 1B and see Methods section in the Supporting Information), with size distributions that did not differ significantly.

Having compared the two preparations by cTCCD, we then turned to a wide-field single-molecule imaging technique, TIRFM, to study the Aβ42–PrP^C interaction on live cells (Figure 2A). We first determined whether the density of Aβ42 species bound to the surface of live cells depends on the density of PrP^C molecules expressed at the cell surface. For this, we used neuroblastoma cells (N2a) that expressed two different levels of PrP^C: cells with endogenous expression ("high" expression) and cells in which PrP^C expression had been reduced by siRNA targeted at PrP^C ("low" expression). We rendered PrP^C at the plasma membrane visible for fluorescence microscopy by addition of the fluorescently labeled anti-PrP^C antibody POM1.[28] Recent work by Sonati et al. showed not only that this antibody does not compete for the putative binding site

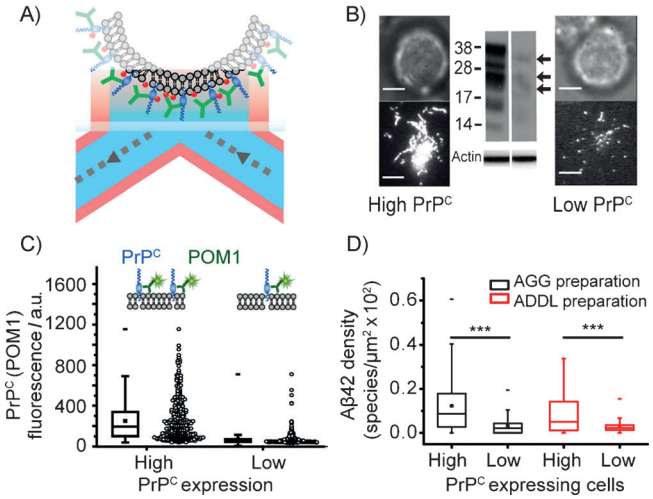

Figure 2. Correlation of Aβ42 and PrP^C densities in the membranes of living cells. **A)** TIRF microscopy of POM1-labeled[28] PrP^C and oAβ42 in the plasma membrane. B) Representative images of cells expressing PrP^C at "high" (left, natural) and "low" (right, PrP^C knockdown) levels at the cell surface. Scale bars: 5 μm. Western blots demonstrating a lower total cellular PrP^C expression; multiple bands (arrows) are different glycosylation states of PrP^C (38 and 28 kDa; mature PrP^C: 27 kDa[29]); actin was used as a loading control. C) Distributions of PrP^C expression in cell membranes as assessed by integrated POM1-Alexa Fluor 488 fluorescence intensities. Each distribution is shown as a box plot (whiskers: 5th and 95th percentiles; –: maximum values) and a scatter plot (each point representing a single cell). PrP^C expression is significantly different for the two cell populations ($median_{high}=193$, $median_{low}=53$, $p=0$ (Mann–Whitney U-test); $n_{high}=426$, $n_{low}=507$). D) Density of Aβ42 species (number/$\mu m^2 \times 10^2$) bound to N2a cells expressing high and low levels of PrP^C (500 nM total peptide; ADDL: $median_{high}=0.05$ and $median_{low}=0.02$, $p_{(ADDL)}=2.2\times10^{-5}$, AGGs: $median_{high}=0.09$ and $median_{low}=0.02$, $p_{(AGG)}=4.4\times10^{-16}$, Mann–Whitney U-test; $n_{(ADDL)}=165$ (high) and 123 (low); $n_{(AGG)}=115$ (high) and 196 (low)). Data were pooled from at least three independent experiments.

of oAβ42, but also that the conformation of the oAβ42 binding domain is unchanged by binding to POM1.[30] Although the same study identified cytotoxic effects elicited by POM1, these occurred on much longer timescales (weeks) than that of our biophysical characterization (hours), so we assume that the oAβ42–PrP^C interactions observed here were unaffected by the presence of POM1. Qualitative analysis by western blotting confirmed that PrP^C expression was substantially suppressed by RNAi (Figure 2B), leading to a ~fourfold decrease in fluorescence intensity from cells labeled with POM1 (Figure 2C). We incubated N2a cells expressing "high" and "low" PrP^C levels with HiLyte Fluor 647-labeled Aβ42, by using the AGG and ADDL protocols to produce mixtures of oligomeric and monomeric Aβ42, exactly as for cTCCD except with dilution to a final concentration of 500 nM (total peptide, equivalent to 5–15 nM oligomer) rather than 25 pM. We then recorded videos to resolve the spatiotemporal coordinates of individual fluorescently labeled Aβ42 species on the cell surface, and then counted the number of species bound to cells in these recordings by using single-particle tracking.[31] This analysis showed that, for both oligomer preparations, the density of Aβ42 species at the surface of N2a cells was decreased 2.5–4.5-fold upon siRNA knockdown of PrP^C expression (Figure 2D), thus suggesting that the majority of oligomers are bound to PrP^C at endogenous expression levels.

Having established a correlation between the density of Aβ42 species bound to the cell membrane and cell-surface PrP^C levels, we used single-particle tracking to detect oAβ42–PrP^C binding at the single-molecule level. We extracted 2D trajectories for diffusing Aβ42 species and PrP^C molecules (POM1) from TIRFM video recordings of cells with "low" PrP^C expression levels; these cells exhibited sufficiently low POM1 densities to enable us to confidently connect corresponding particle images in successive frames by using a nearest-neighbor algorithm (Figure 3A, top and middle panels; Supporting Videos 1 and 2).[32,33] We identified PrP^C–oAβ42 complexes as POM1 trajectories that spatially and temporally overlapped (i.e. colocalized) with the trajectory of an Aβ42 oligomer (Figure 3A, B bottom panels; colocalization criteria and representative trajectories in the Experimental Section and Figures S1–S3; see also ref. [34]). Because the diffusion of receptors in the cell membrane is a stochastic process, the probability of two unassociated molecules moving on a similar trajectory (and within a short distance of one another) is very low on typical timescales (ms) of single-particle tracking. Hence, in contrast to bulk colocalization measurements, the number of chance coincidence events detected is greatly reduced. Nevertheless, we addressed this quantitatively by estimating the chance overlap of trajectories by repeating the colocalization analysis after spatial shuffling (i.e. inverting the image axes: $x \rightarrow y$ and $y \rightarrow x$ for one channel), thus enabling correction of all colocalization measurements for chance coincidence (Table S1). Prior to investigation of the PrP^C–oAβ42 complexes, we evaluated the dynamic range for our approach by measuring the extent of colocalization for a positive control. We recorded videos resolving the diffusion of dual-labeled PrP^C receptors on N2a cells by incubating them with both Alexa Fluor 647-labeled POM1 and Alexa Fluor 488-labeled POM3 (Figure S4);

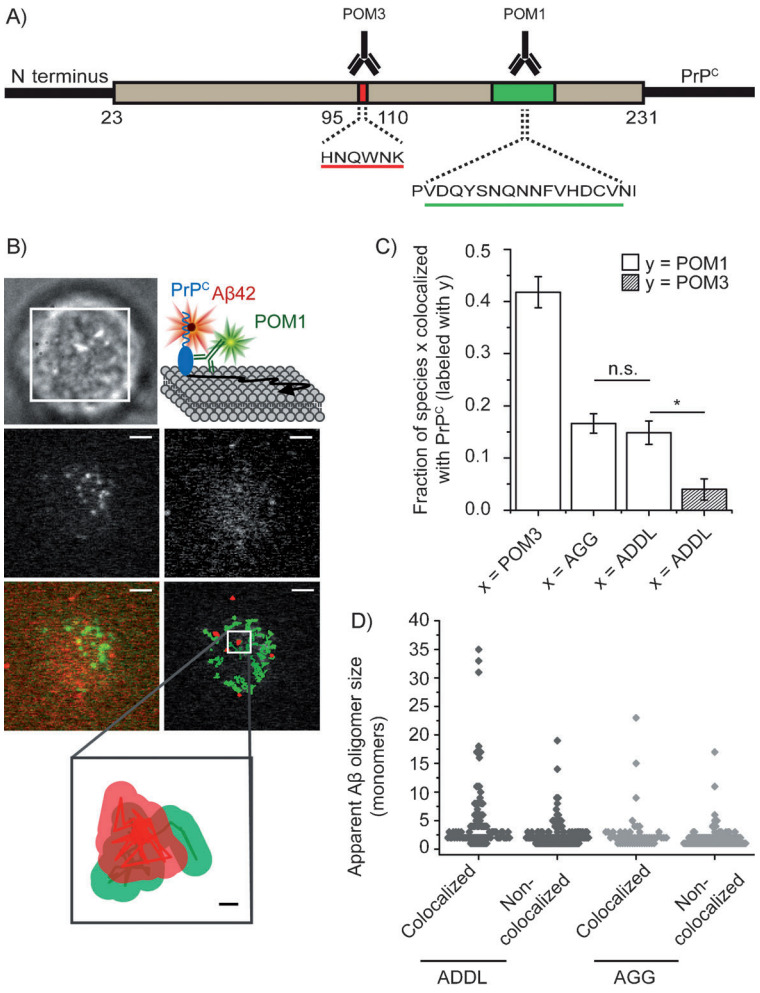

Figure 3. Characterization of the oligomerization order of Aβ42 bound to PrP^C and other membrane components by TIRFM and single-particle tracking. A) Epitopes recognized by anti-PrP^C antibodies (POM antibodies). Laurén et al.[9] have mapped the binding site of Aβ to residues 95–110, so POM1 can be assumed to bind PrP^C independent of any Aβ present, whereas POM3 and Aβ compete for the same epitope. B) Single-molecule imaging of PrP^C and oAβ42 diffusing in live cell membranes. From left to right, first row: phase contrast image of an N2a cell; the white frame corresponds to the region shown in the second and third rows; second row: frame taken from a video showing POM1 antibody bound PrP^C (left) and HiLyte Fluor 647-labeled Aβ42 oligomers (right); third row: color overlay of two channels for the frame above, and color overlay of trajectories (scale bars: 2 μm). Below: expansion of two colocalized trajectories; the shaded regions correspond to the uncertainty of particle localization (scale bar: 100 nm). C) Extent of colocalization of PrP^C-binding antibodies and Aβ42 oligomers, corrected for chance coincidence; ($p_{(n.s.)} = 0.50$, p* = 0.01, two-sample t-test, unequal variance assumed). Error bars are SEM. D) Apparent Aβ42 oligomer size distributions for species colocalized, or not, with PrP^C by using the fluorescence intensity of the detected Aβ42 species as an indicator of oligomer size (for details see text); $\text{median}_{(ADDL)} = 3$ (bound) and 2 (unbound), $\text{median}_{(AGG)} = 2$ (bound) and 1 (unbound); $n_{(ADDL)} = 99$ (bound) and 174 (unbound), $n_{(AGG)} = 48$ (bound) and 112 (unbound).

these antibodies target different epitopes on PrP^C and can therefore simultaneously bind to a single receptor (Figure 3A). We analyzed the POM1 and POM3 trajectories for their spatiotemporal coincidence, and found colocalized fractions of POM1 and POM3 of 0.39 ± 0.05 and 0.42 ± 0.03, respectively (Figure 3C and Table S1). Although theoretically 100% of these trajectories should be colocalized, experimentally obtained values are typically much lower for single-molecule measurements due to dissociation of the antibodies and the fact that some trajectories are not detected because of limited signal and fluorophore photobleaching and blinking.[34] Confident that our method was able to detect colocalization at the single-molecule level, we analyzed the degree of colocalization for trajectories extracted from videos to resolve the diffusion of individual POM1-labeled PrP^C receptors and oAβ42 molecules. We found that approximately 3% of PrP^C receptors colocalized with oAβ42, possibly due to substantial dissociation of the complexes prior to recording, whereas 17 ± 2% (AGG) and 15 ± 2% (ADDL) of all Aβ42 oligomers bound to the cell membrane were coincident with the trajectory of a PrP^C receptor (Figure 3C). We note that previous investigations (using different cell lines) reported similarly small fractions of PrP^C-bound Aβ42 (~38%,[9] <11%),[35] a result of oligomers binding to other membrane components in addition to PrP^C. In the presence of the competitive antibody POM3, colocalization of oAβ42 with PrP^C was reduced approximately fourfold (Figure 3C). As POM3 recognizes an epitope (Figure 3A)[28] that overlaps the putative oAβ42 binding site of PrP^C,[9] this provides strong support that colocalization is attributable to a specific molecular interaction between PrP^C and Aβ42.

In order to establish the oligomerization order of the Aβ42 species bound to PrP^C and to allow comparison with oligomers bound to other membrane components, we extracted the fluorescence intensity of each of the detected Aβ42 species following colocalization classification.[31,36] These fluorescence intensities were normalized according to the mean step size of photobleaching traces recorded for monomeric Aβ42 (intensity analysis in the Experimental Section; representative photobleaching traces in Figure S5). This analysis showed the median size of a bound oligomer to be approximately a trimer for the ADDL preparation and a dimer for AGG (Figure 3D). It is noteworthy that the large interquartile range of fluorescence intensities indicates that some of the PrP^C-bound oAβ42 species were much larger than a dimer (maximum ~35-mer (ADDL), 20-mer (AGG)).

In summary, this work confirms that there is a specific interaction between oAβ42 and PrP^C at the surface of neuronal cells and establishes that the majority of PrP^C-bound oAβ42 species are small oligomers. The size distribution of oAβ42 associated with PrP^C therefore reflects that found in the aggregated mixtures incubated with the cells. This observation was independent of the oAβ42 preparation method, thus suggesting that two commonly used protocols yield oligomers of similar sizes and similar affinities for PrP^C. The question of which sizes of oAβ42 interact most strongly with PrP^C has so far elicited contradictory answers: Larson et al. found that endogenous PrP^C extracted from brain tissue is bound exclusively to dimeric Aβ42,[35] whereas Nicoll et al. suggested that much larger species bind most avidly.[37] The latter conclusion was based on the observation that the abundance of Aβ nanotubes in aggregating mixtures correlated with increased occupancy of PrP^C in ELISA measurements. However, the different results are not necessarily inconsistent, given that the appearance of protofibrils in an aggregating mixture is accompanied by an increase in the concentration of small oAβ42. This would lead to an overall increase in binding affinity of the preparation for PrP^C, even if protofibrilar species are not major players in the binding process. Our data shed further light on this controversy. We found that Aβ42 species bound to PrP^C at the cell membrane are indeed predominantly small oligomers (median size estimated to be dimers to trimers), but we also observed binding of oAβ42 species with sizes up to 35-mers (i.e., protofibrilar oAβ42).[38,39] With the caveat that the requirement for removal of excess oAβ42 means that our single-molecule imaging was not carried out at equilibrium, our data support a scenario in which the majority of PrP^C-bound Aβ42s on neuronal membranes are small oligomers, with only a minor contribution from protofibrils. Single-molecule biophysical studies of the type described here thus constitute a useful tool to characterize the Aβ species that interact with specific receptors, without the need for isolation or stabilization of species of a specific size.

Experimental Section

Cell culture: Neuroblastoma 2a cells (N2a, ECACC 89121404) were cultured in DMEM (Invitrogen/Life Technologies) supplemented with fetal calf serum (10%, FCS; Sigma–Aldrich) and penicillin/streptomycin (1%) in 5% CO_2 at 37 °C.

RNA interference: ON-TARGETplus SMART pool siRNA containing four siRNA sequences designed to target mouse PrP (Dharmacon/Thermo Scientific) was used for PrP knockdown, with DharmaFECT D1 (Dharmacon/Thermo Scientific) as the cellular transfection reagent. Prior to the transfection, N2a cells were seeded in six-well NUNC plates (200000 cells per well). A stock solution of siRNA (200 μM in RNase-free water) was incubated at 25 °C for 5–10 min; the RNA concentration was determined by absorbance at 260 nm. In order to perform the knockdown, the siRNA stock was diluted 100-fold in Gibco Opti-MEM medium (Life Technologies) and mixed (5 μL) with transfection reagent (30 μL). This mixture was incubated for 20 min at 25 °C before diluting twofold in DMEM and addition to the plated cells. The final concentration of siRNA in each well was 500 nM, and the cells were incubated for a further 48 h at 37 °C prior to sample preparation for imaging. Immunoblotting was used to confirm that PrP^C expression was indeed reduced in the N2a cells after incubation with siRNA.

Preparation of Aβ42 (AGG) oligomers: Monomeric solutions of Aβ42 singly labeled with either HiLyte Fluor 488 or HiLyte Fluor 647 were obtained by dissolving each lyophilized peptide (AS-60479-01 or AS-64161, Anaspec, Fremont, CA) in NaOH (0.01 M) and sonication on ice for 30 min (Sonorex; Bandelin, Berlin, Germany).[26] Aliquots of the peptide solutions were flash frozen and stored at −80 °C. The concentration of each labeled peptide was measured by using confocal single-molecule spectroscopy as described previously.[24] Prior to each aggregation, the peptide solutions were brought to pH 7.4 by diluting to 10 μM in SSPE buffer

(sodium phosphate (10 mM, pH 7.4) with NaCl (150 mM) and Na_2EDTA (10 mM)). Oligomers were prepared by incubating these solutions for 1 h at 37 °C. For characterization by cTCCD, equimolar mixtures of HiLyte Fluor 488- and 647-labeled peptide were aggregated and diluted (25 pM total peptide) directly before measurement, as previously described.[24] For characterization of oAβ42–PrP^C interactions by TIRFM, Aβ42 labeled solely with HiLyte Fluor 647 was aggregated and diluted (500 nM total peptide) before adding to N2a cells. Although we used different peptide concentrations for cTCCD and TIRFM, previous work has shown that the oligomers are stable over the time taken for the measurements,[24] so we assume the same oligomer size distributions are present in both types of experiment.

Preparation of Aβ42 (ADDL) oligomers: Aβ42 (ADDL) oligomers were prepared by using the protocol described by Laurén and coworkers[9] with minor modifications: peptides were singly labeled with either HiLyte Fluor 488 or HiLyte Fluor 647 instead of biotin, and the aggregation concentration was 40 instead of 100 μM, as low yields were obtained from the starting material. As for the AGG preparation, equimolar mixtures of HiLyte Fluor 488- and 647-labeled peptides were aggregated and diluted to 25 pM directly before characterization by cTCCD; Aβ42 labeled solely with HiLyte Fluor 647 was aggregated and diluted to 500 nM before adding to N2a cells.

Sample preparation for imaging: N2a cells were seeded in Nunclon Delta-treated six-well plates (Thermo Scientific) 48 h prior to experiments, and treated with siRNA as described above if required. Before imaging, cells were incubated with sterile PBS (12 min, 37 °C) to ease detachment from the surface by aspirating with a pipette. Cells (~10^6) were suspended in DMEM and incubated in a microcentrifuge tube with solutions of oligomeric Aβ42 (prepared as described above; final concentrations as in the text) and either POM 1 (5 nM) or POM 3 antibodies (1 nM) for 30 min at 4 °C. Cells were then washed with DMEM (×3) and PBS (×1) with centrifugation (600 *g*, 2 min) and resuspension of the pellet, and transferred to glass cover slips for imaging. Cover slips were cleaned with Piranha solution (sulfuric acid/hydrogen peroxide, 3:1) as described previously,[31] thoroughly rinsed with ultrapure water (MilliQ, 18.2 MΩ), exposed to oxygen plasma for 2 min (Femto Plasma Cleaner; Diener Electronic, Royal Oak, MI, USA), and subsequently coated with a solution of PLL(20)-g[3.7]-PEG(2.3)/PEG(3.4)-RGD (12%) (PLL-PEG-RGD, 1 mg mL^{-1}; SuSoS AG, Dübendorf, Switzerland) for 10 min at room temperature.[31] The slides were transferred to the microscope stage, cells were added and allowed to settle for 5 min, then imaged at room temperature within 20 min of cell attachment.

TIRFM measurements: Imaging was performed by using total internal reflection fluorescence microscopy (TIRFM). A HeNe laser (633 nm; 25-LHP-991(230), Melles Griot, Carlsbad, CA) and a diode laser (488 nm; PC13589, Cyan Scientific, Spectra Physics, Santa Clara, CA) were directed into a TIRF objective (60× Plan Apo TIRF, NA 1.45; Nikon) mounted on an Eclipse TE2000-U microscope (Nikon) parallel to the optical axis and offset in order to achieve total internal reflection of the beam. The emitted fluorescence was collected by the same objective and separated from the returning TIR beam by a dichroic mirror (FF500/646-Di01; Semrock, Rochester, NY). Green and red fluorescence emissions were separated by a second dichroic mirror and filter sets (585 DXLR, HQ525/50 (green emission), QMax/EM670-750 (red emission); Omega Optical, Brattleboro, VT) with a Dual-View imaging system (Photometrics, Tucson, AZ). The fluorescence signals from both channels were simultaneously recorded at −70 °C with a Cascade II:512 EMCCD camera (Photometrics); each color was recorded on separate halves of the EMCCD chip. Data were acquired at 28.6 frames per second with Micro-Manager.[40]

Image analysis: Custom-written MATLAB software (R2011b, MathWorks, Natick, MA) was used to analyze the image data. After manual selection of the cell area based on bright-field images acquired during the data collection phase, the fluorescence images corresponding to the selected cells were band-pass filtered to remove the low-frequency modulated background and high-frequency camera noise typically in our image data. The implemented filtering algorithm (bpass.m, David G. Grier, University of Chicago) was converted to MATLAB format by Eric Dufresne (Yale University) and is freely available online (http://physics.georgetown.edu/matlab/index.html, accessed Oct 2014). As the endogenous density of PrP^C receptors in the plasma membrane of N2a cells was too high for reliable detection of individual fluorescent signals, the mean fluorescence intensity for whole cells was calculated. As the observed area of the cell membrane was considerably smaller than the area selected from the bright-field image (20–25%), the mean intensity value was only calculated from pixels whose intensities were larger than the sum of the mean intensity and three standard deviations of the total area selected. For cells expressing "low" levels of PrP^C, individual spots could be resolved, and detection and sequential linkage of the detected individual receptor positions in subsequent frames was performed as previously described.[31,32] Briefly, from the positions of each particle in each frame obtained from spot detection, corresponding particles were linked by using custom-written MATLAB code and an implementation of the particle-tracking function of Crocker and Grier [33] written in Interactive Data Language (IDL; Exelis Visual Information, Boulder, CO) The mean nearest-neighbor distance between tracked particles within a recording was 350–500 nm.

Calculation of localization precision: In order to determine the localization precision of the imaging system, HiLyte Fluor 647-labeled Aβ42 and 488-labeled POM1 solutions were diluted (1 nM in PBS) and adsorbed onto a cleaned glass cover-slip for imaging. The data obtained were used to calculate the localization precision by determining the positions of the fluorescently labeled species as previously described.[32] Each particle's central position was plotted over time, and the standard deviation (representing particle localization precision) was calculated (Figure S1). This gave similar precisions (σ) for each color: 43.8 ± 21.4 nm (green channel, POM1, n = 96) and 41.2 ± 15.3 nm (red channel, Aβ42, n = 1514).

Determination of channel registration for dual-color imaging: A grid of regularly spaced, ion-beam-etched holes in gold-on-glass was used to achieve image registration across both emission channels. The Dual-View optics were adjusted to maximize the overlap of the grid images in the two channels under bright-field illumination (95% of the positions were in alignment with a precision of ±146 nm; Figure S2).

Determination of coincidence criterion: We obtained the colocalization criterion from the RMS deviations in the positional accuracies for green- and red-emitting molecules [Eq. (1)]

$$\sigma_{mean} = \sqrt{\sigma_{488}^2 + \sigma_{647}^2} \quad (1)$$

Equation (1) with our positional accuracies (calculated above) gave a value of 60.1 ± 26.3 nm. Hence, in order to obtain a 95% probability of colocalization, the distance threshold is 2σ (corresponding to ~120 nm). Adding the value for our image registration accuracy (see TIRFM Experimental Setup "Determination of channel registra-

tion" above), gives a colocalization distance value:

$$\sigma_{calcd} = \sqrt{(120\ nm)^2_{localization\ on\ precision} + (146\ nm)^2_{image\ registration}} = 189\ nm \quad (2)$$

For this work we chose a colocalization distance of 200 nm, in order to minimize the chance of missing associated molecules.

Calculation of trajectory coincidence: After the trajectories had been identified, we examined association by applying a nearest-neighbor distance approach.[34] For each pair of fluorescence trajectories, the distances between their positions in corresponding frames were calculated; two molecules were considered associated if their tracked positions remained within 200 nm (colocalization criterion) for eight or more frames (>0.28 s), thus obtaining $n_{colocalized\ (PrPC,A\beta)}$. To examine the contribution of chance coincidence, we repeated this colocalization analysis for spatially decoupled trajectory pairs; for this, the coordinates of one of the trajectories was rotated 90° prior to analysis ($x \rightarrow y$ and $y \rightarrow x$), thus obtaining $n_{colocalized\ (PrPC,A\beta),chance}$. The overall coincidence (of Aβ42 with PrP^C) corrected for chance coincidence events was taken to be

$$fraction_{coincidence,PrP} = \frac{n_{colocalized(PrP,A\beta)} - n_{colocalized(PrP,A\beta),chance}}{total\ number\ of\ tracks(A\beta) - n_{colocalized(PrP,A\beta),chance}} \quad (3)$$

This coincidence value was calculated for each data set (from all events across every video taken); reported values are mean ± SD ($n \geq 3$).

Estimation of oligomerization order of Aβ42 colocalized with PrP^C: The intensity of each Aβ42 trajectory was averaged over multiple frames before bleaching, that is, before the intensity of the particle in frame $n+1$ dropped below 60% the intensity of the particle in frame n. Oligomer sizes were estimated from the intensities as described previously by using monomer intensities derived from the bleaching step size of immobilized Aβ42 monomers under identical illumination conditions.[31]

Statistical methods: All statistical analysis was performed in Origin 8 (OriginLab Corp., Northampton, MA). To assess differences between sets of non-normally distributed data sets, Mann–Whitney U-tests were used; two-sample Student t-tests and one-factor ANOVA tests were used for small data sets ($n < 10$).

Acknowledgements

K.A.G. was supported by fellowships from the Engineering and Physical Sciences Research Council (EPSRC) and Studienstiftung des deutschen Volkes. P.N. was supported by a Marshall Scholarship from the Marshall Aid Commemoration Commission and a Graduate Research Fellowship from the National Science Foundation. L.W. was supported by an EPSRC fellowship. The research of S.Q., D.K., P.S.G.H. and C.M.D. is supported by the Wellcome Trust and that of D.K. by the Augustus Newman Foundation.

Keywords: amyloid beta-peptides · biophysics · neurochemistry · protein aggregation · single-molecule studies

[1] M. Bucciantini, E. Giannoni, F. Chiti, F. Baroni, L. Formigli, J. S. Zurdo, N. Taddei, G. Ramponi, C. M. Dobson, M. Stefani, *Nature* **2002**, *416*, 507–511.
[2] F. Chiti, C. M. Dobson, *Annu. Rev. Biochem.* **2006**, *75*, 333–366.
[3] D. M. Walsh, I. Klyubin, J. V. Fadeeva, W. K. Cullen, R. Anwyl, M. S. Wolfe, M. J. Rowan, D. J. Selkoe, *Nature* **2002**, *416*, 535–539.
[4] N. Arispe, E. Rojas, H. B. Pollard, *Proc. Natl. Acad. Sci. USA* **1993**, *90*, 567–571.
[5] J. C. Diaz, O. Simakova, K. A. Jacobson, N. Arispe, H. B. Pollard, *Proc. Natl. Acad. Sci. USA* **2009**, *106*, 3348–3353.
[6] R. Kayed, A. Pensalfini, L. Margol, Y. Sokolov, F. Sarsoza, E. Head, J. Hall, C. Glabe, *J. Biol. Chem.* **2009**, *284*, 4230–4237.
[7] D. Westaway, J. H. Jhamandas, *Prion* **2012**, *6*, 359–363.
[8] T. Kim, G. S. Vidal, M. Djurisic, C. M. William, M. E. Birnbaum, K. C. Garcia, B. T. Hyman, C. J. Shatz, *Science* **2013**, *341*, 1399–1404.
[9] J. Laurén, D. A. Gimbel, H. B. Nygaard, J. W. Gilbert, S. M. Strittmatter, *Nature* **2009**, *457*, 1128–1232.
[10] C. Balducci, M. Beeg, M. Stravalaci, A. Bastone, A. Sclip, E. Biasini, L. Tapella, L. Colombo, C. Manzoni, T. Borsello, R. Chiesa, M. Gobbi, M. Salmona, G. Forloni, *Proc. Natl. Acad. Sci. USA* **2010**, *107*, 2295–2300.
[11] S. Chen, S. P. Yadav, W. K. Surewicz, *J. Biol. Chem.* **2010**, *285*, 26377–26383.
[12] A. M. Calella, M. Farinelli, M. Nuvolone, O. Mirante, R. Moos, J. Falsig, I. M. Mansuy, A. Aguzzi, *EMBO Mol. Med.* **2010**, *2*, 306–314.
[13] D. B. Freir, A. J. Nicoll, I. Klyubin, S. Panico, J. M. Mc Donald, E. Risse, E. A. Asante, M. A. Farrow, R. B. Sessions, H. R. Saibil, A. R. Clarke, M. J. Rowan, D. M. Walsh, J. Collinge, *Nat. Commun.* **2011**, *2*, 336.
[14] H. W. Kessels, L. N. Nguyen, S. Nabavi, R. Malinow, *Nature* **2010**, *466*, E3–E4.
[15] W. Kudo, H.-P. Lee, W.-Q. Zou, X. Wang, G. Perry, X. Zhu, M. A. Smith, R. B. Petersen, H.-g. Lee, *Hum. Mol. Genet.* **2012**, *21*, 1138–1144.
[16] U. K. Resenberger, A. Harmeier, A. C. Woerner, J. L. Goodman, V. Müller, R. Krishnan, R. M. Vabulas, H. A. Kretzschmar, S. Lindquist, F. U. Hartl, G. Multhaup, K F. Winklhofer, J. Tatzelt, *EMBO J.* **2011**, *30*, 2057–2070.
[17] D. Rial, F. S. Duarte, J. C. Xikota, A. E. Schmitz, A. L. Dafré, C. P. Figueiredo, R. Walz, R. D. S. Prediger, *Neuroscience* **2009**, *164*, 896–907.
[18] M. Cissé, P. E. Sanchez, D. H. Kim, K. Ho, G.-Q. Yu, L. Mucke, *J. Neurosci.* **2011**, *31*, 10427–10431.
[19] D. A. Gimbel, H. B. Nygaard, E. E. Coffey, E. C. Gunther, J. Laurén, Z. A. Gimbel, S. M. Strittmatter, *J. Neurosci.* **2010**, *30*, 6367–6374.
[20] E. Saijo, S. W. Scheff, G. C. Telling, *Prion* **2011**, *5*, 109–116.
[21] G. Forloni, A. Sclip, T. Borsello, C. Balducci, *Prion* **2013**, *7*, 60–65.
[22] I. Benilova, B. De Strooper, *Science* **2013**, *341*, 1354–1355.
[23] S. E. Lesné, *Int. J. Cell Biol.* **2013**, *2013*, 950783.
[24] P. Narayan, A. Orte, R. W. Clarke, B. Bolognesi, S. Hook, K. A. Ganzinger, S. Meehan, M. R. Wilson, C. M. Dobson, D. Klenerman, *Nat. Struct. Mol. Biol.* **2012**, *19*, 79–83.
[25] H. Ding, P. T. Wong, E. L. Lee, A. Gafni, D. G. Steel, *Biophys. J.* **2009**, *97*, 912–921.
[26] D. B. Teplow, *Methods Enzymol.* **2006**, *413*, 20–33.
[27] M. P. Lambert, A. K. Barlow, B. A. Chromy, C. Edwards, R. Freed, M. Liosatos, T. E. Morgan, I. Rozovsky, B. Trommer, K. L. Viola, P. Wals, C. Zhang, C. E. Finch, G. A. Krafft, W. L. Klein, *Proc. Natl. Acad. Sci. USA* **1998**, *95*, 6448–6453.
[28] M. Polymenidou, R. Moos, M. Scott, C. Sigurdson, Y. Shi, B. Yajima, I. Hafner-Bratkovič, R. Jerala, S. Hornemann, K. Wüthrich, A. Bellon, M. Vey, G. Garen, M. N. G. James, N. Kav, A. Aguzzi, *PLoS One* **2008**, *3*, e3872.
[29] A. Ashok, R. S. Hegde, *PLoS Pathog.* **2009**, *5*, e1000479.
[30] T. Sonati, R. R. Reimann, J. Falsig, P. K. Baral, T. O'Connor, S. Hornemann, S. Yaganoglu, B. Li, U. S. Herrmann, B. Wieland, M. Swayampakula, M. H. Rahman, D. Das, N. Kav, R. Riek, P. P. Liberski, M. N. G. James, A. Aguzzi, *Nature* **2013**, *501*, 102–106.
[31] P. Narayan, K. A. Ganzinger, J. McColl, L. Weimann, S. Meehan, S. Qamar, J. A. Carver, M. R. Wilson, P. St George-Hyslop, C. M. Dobson, D. Klenerman, *J. Am. Chem. Soc.* **2013**, *135*, 1491–1498.
[32] L. Weimann, K. A. Ganzinger, J. McColl, K. L. Irvine, S. J. Davis, N. J. Gay, C. E. Bryant, D. Klenerman, *PLoS One* **2013**, *8*, e64287.
[33] J. C. Crocker, D. G. Grier, *J. Colloid Interface Sci.* **1996**, *179*, 298–310.
[34] P. D. Dunne, R. A. Fernandes, J. McColl, J. W. Yoon, J. R. James, S. J. Davis, D. Klenerman, *Biophys. J.* **2009**, *97*, L5–L7.

[35] M. Larson, M. A. Sherman, F. Amar, M. Nuvolone, J. A. Schneider, D. A. Bennett, A. Aguzzi, S. E. Lesné, *J. Neurosci.* **2012**, *32*, 16857 – 16871.
[36] J. A. Schauerte, P. T. Wong, K. C. Wisser, H. Ding, D. G. Steel, A. Gafni, *Biochemistry* **2010**, 49, 3031 – 3039.
[37] A. J. Nicoll, S. Panico, D. B. Freir, D. Wright, C. Terry, E. Risse, C. E. Herron, T. O'Malley, J. D. F. Wadsworth, M. A. Farrow, D. M. Walsh, H. R. Saibil, J. Collinge, *Nat. Commun.* **2013**, *4*, 2416
[38] J. D. Harper, S. S. Wong, C. M. Lieber, P. T. Lansbury, Jr., *Chem. Biol.* **1997**, *4*, 119 – 125.
[39] A. Jan, D. M. Hartley, H. A. Lashuel, *Nat. Protoc.* **2010**, *5*, 1186 – 1209.
[40] A. Edelstein, N. Amodaj, K. Hoover, R. Vale, N. Stuurman, in *Current Protocols in Molecular Biology,* Wiley, New York, **2010**.

Received: July 14, 2014
Published online on October 7, 2014